J Mater Sci (2010) 45:4431–4438
DOI 10.1007/s10853-010-4525-1

Fabrication of AA6061/Al_2O_3 nano ceramic particle reinforced composite coating by using friction stir processing

Min Yang · Chengying Xu · Chuansong Wu · Kuo-chi Lin · Yuh J. Chao · Linan An

Received: 23 September 2009 / Accepted: 13 April 2010 / Published online: 29 April 2010

Abstract Nano ceramic particle reinforced composite coatings were created by incorporating Al_2O_3 ceramic particles into the surface of AA6061-T6 alloy plate with multiple pass friction stir processing (FSP). Optical microscopy and Micro-Vickers hardness tests were employed to investigate the influence of axial force and the number of FSP pass on the distribution of the ceramic particles and the hardness of the generated nano ceramic particle reinforced composite coating. Results show that the composite coating is as deep as the length of the pin probe. No distinct interface was developed between the coating and the base metal. The composite region becomes greater as the axial force and the number of FSP pass increased. At the same time, the distribution of the ceramic particles became more homogeneous. Nano particles in the coating have no significant effect on the macro-hardness of AA6061-T6 aluminum alloy even in the composite zone due to the softening of matrix material resulted from overaging. Spindle torque of the tool increased with increasing axial force, while it became less variable and smaller in subsequent pass compared to that in the first pass.

M. Yang (✉) · C. Wu
Key Laboratory of Liquid Structure and Heredity of Materials (Ministry of Education), Shandong University, No. 73 Jingshi Road, Jinan 250061, Shandong, People's Republic of China
e-mail: miny@sdu.edu.cn

C. Xu · K. Lin · L. An
Department of Mechanical, Materials and Aerospace Engineering, Advanced Materials Processing and Analysis Center, University of Central Florida, Orlando, FL 32816, USA

Y. J. Chao
Department of Mechanical Engineering, University of South Carolina, 300 Main Street, Columbia, SC 29208, USA

Introduction

Aluminum alloys are very promising for structural applications in aerospace, military, and transportation industries due to their light weight, high strength-to-weight ratio, and resistance to corrosion. However, the application of the materials is significantly limited by their poor wear resistance, manifested by severe adhesive wear. In comparison with the unreinforced aluminum alloys, aluminum matrix composites reinforced with ceramic phases exhibit higher strength and stiffness, improved tribological characteristics, and increased resistance to creep and fatigue. Moreover, recent report reveals that the metal matrix composites reinforced by nano-sized ceramic powder exhibit superior wear resistance by having significantly low wear rates and desired abrasive wear. However, these composites also suffer from a great loss in ductility, toughness and thermal conductivity.

For applications where surface contact is involved, the useful life of components is mainly determined by their surface properties such as wear resistance. Therefore, it is highly desirable that only the surface layer of the component is reinforced by nano ceramic phases while the bulk of the component still maintains the original structure with good ductility and thermal conductivity [1–4].

Existing processing technologies used for creating metal matrix composite coating include thermal spraying, laser cladding, surface alloying by using lasers or high energy electron beam or plasma arcs [5–8]. In these cases, it is difficult to avoid interfacial reactions between the reinforcement phases and the metal matrix, growth of nano particles, and/or formation of certain unintended and detrimental phases. The electro-deposit and cold spraying methods have also been applied to obtain nano-composite coatings. But the composite coatings present aggregation of reinforcement particles and low density [9, 10].

Friction stir processing (FSP) has been demonstrated as an effective tool for enhancing metal properties through modifying the microstructures of the working piece. FSP is based on the friction stir welding (FSW) technique invented by The Welding Institute (TWI) in 1991. Recently, attention has been attracted to employ FSP to incorporate ceramic particles into surface layer of aluminum or magnesium to form surface composite [11–23]. Mishra and coworkers [11–14] pre-placed micrometer-sized ceramic powder on aluminum alloy surface to create metal matrix composite by one pass and found that the volume fraction of particles was uncontrollable. The other researchers [15–23] applied FSP to incorporate nano-sized ceramic particles into aluminum or magnesium alloy to fabricate composite by one or multiple passes. In spite of these efforts, detailed studies on friction stir processing have not been reported.

In this article, we report a detailed study on using FSP to form nanocomposite surface layer on bulk AA6061 aluminum alloy. 6XXX series alloys have good formability, machinability, and corrosion resistance, and are extensively employed in marine frames, pipelines, storage tanks, and aircraft structures [24]. This article focuses on the effect of FSP axial force and number of overlapped pass on the applied torque, reinforcement phase distribution, and hardness of composite coatings.

Experimental procedure

The powder used in this study was the commercially available Al_2O_3 powder (99.9% purity and 50 nm average particle size). The rolled plates of 10 mm thick, AA6061 aluminum alloy, was cut into the desired size of 300 × 150 mm by water jet. Holes with 2 mm in diameter and 2 mm in depth were drilled by numerically controlled drilling machine. The layout and the spacing between the holes as well as the dimensions of the plate are schematically shown in Fig. 1. The surface of the aluminum alloy plate was cleaned first. Al_2O_3 powder mixed with small amount of methanol was then filled into the holes of the plates. The aluminum plate with pre-placed Al_2O_3 particles in the holes was finally subjected to friction stir processing after drying in air.

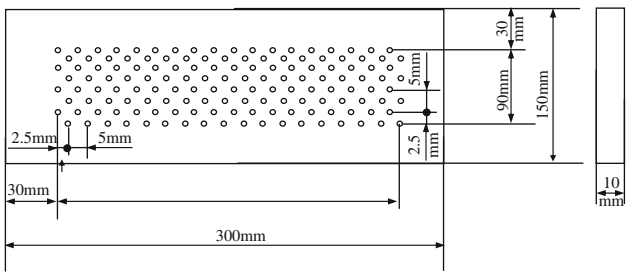

Fig. 1 Arrangement of holes on the plate for filling the nano Al_2O_3 particles

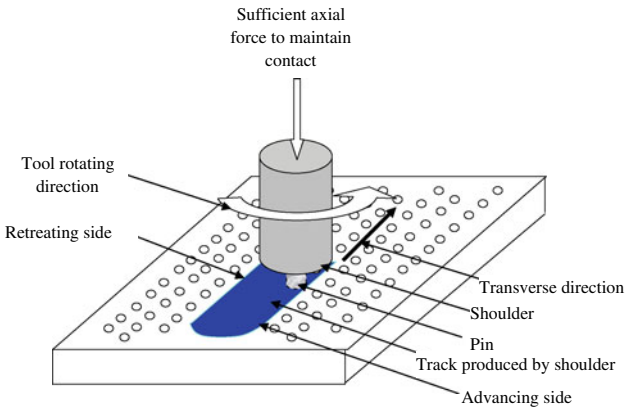

Fig. 2 Schematic of the FSP process

An FSP is schematically shown in Fig. 2. FSP was conducted using an MTS friction stir welding system. The pin of the tool is 10 mm in diameter and 3 mm in length, with a shoulder diameter of 27 mm. The profile of the pin is three flat sided. During FSP, both of the transverse speed, 203.2 mm/min, and the rotational speed, 480 rpm, of the tool were kept constant in this study. Without interference to each other, the FSP was conducted on three paths (denoted as Path 1 to Path 3) sequentially on the same plate as shown in Fig. 3. Path 1 and Path 2 had three passes and Path 3 had two passes of the FSP (see Table 1). The direction of all passes was from the left to the right in the configuration shown in Fig. 3. The axial force varied from 13.23 to 22.05 kN (see Table 1).

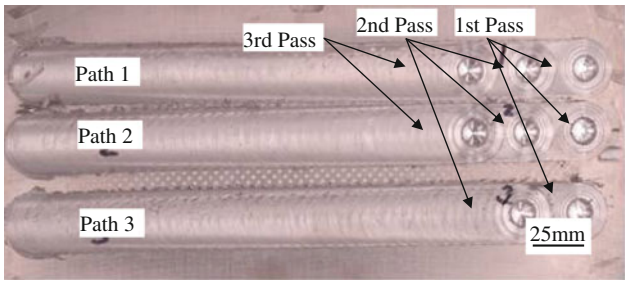

Fig. 3 Picture of as-processed plate with three paths—Path 1 and Path 2 have three passes and Path 3 has two passes only

Table 1 Axial force (kN) measured from the friction stir processing in this study

	Path 1	Path 2	Path 3
1 Pass	17.64	13.23	13.23
2 Pass	17.64	17.64	22.05
3 Pass	17.64	22.05	

After the FSP, the particle distribution of specimens was examined by optical microscopy (OM) without etching. The specimens for metallographic examination were sectioned from as-processed aluminum plates and polished using different grades of emery papers. Final polishing was done using the diamond compound (1 μm particle size) in disk polishing machine. The micro-hardness testing of composite coating and aluminum alloy substrate was conducted by a Micromet, Buehler Ltd. Micro-hardness tester at a 500 g load for 15 s. The spindle torque of the rotating tool during the FSP was recorded by Datum Electronic Torque Log Software with the MTS machine in real time.

Results and discussion

Macrostructure

Optical microscopic examinations revealed that both the number of FSP pass and axial force have significant effects on the formation of composite coating. There are different regions in the FSP processed samples as shown in Fig. 4, which is from a cross section of the sample perpendicular to the FSP pass. The regions include (a) unaffected base metal, (b) heat affected zone (HAZ), (c) thermo-mechanically affected zone (TMAZ), (d) friction stir zone (FSZ), (e) aluminum matrix composites zone (AMCZ), and (f) unmixed Al_2O_3 ceramic powder.

The low magnification OM images of the cross section of the FSP samples from different path are shown in Fig. 5. The retreating side is on the left while the advancing side is on the right of the image. Note that in each path the length of the pass after the first was shortened as compared to the previous one, so cross sections experiencing different pass from the same path can be harvested for investigation. The location of each specimen cut from the original plate for cross section examination is depicted in Fig. 5a. The OM images in Fig. 5 indicate that the AMCZ appeared at the advancing side first, and then expanded from the advancing side to the retreating side after additional pass(es). The

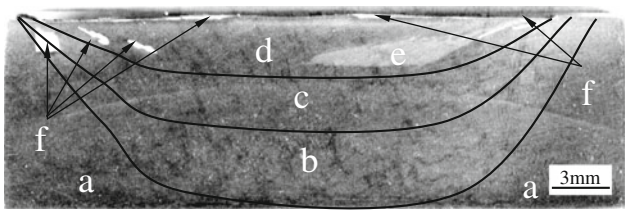

Fig. 4 Typical regions in an FSP processed sample (this cross section is from Path 2 processed after one pass and perpendicular to the FSP pass); *a* Unaffected Base Metal, *b* Heat Affected Zone (HAZ), *c* Thermo-Mechanically Affected Zone (TMAZ), *d* Friction stir zone (FSZ), *e* Aluminum Matrix Composites Zone (AMCZ), and *f* Unmixed Al_2O_3 ceramic powder

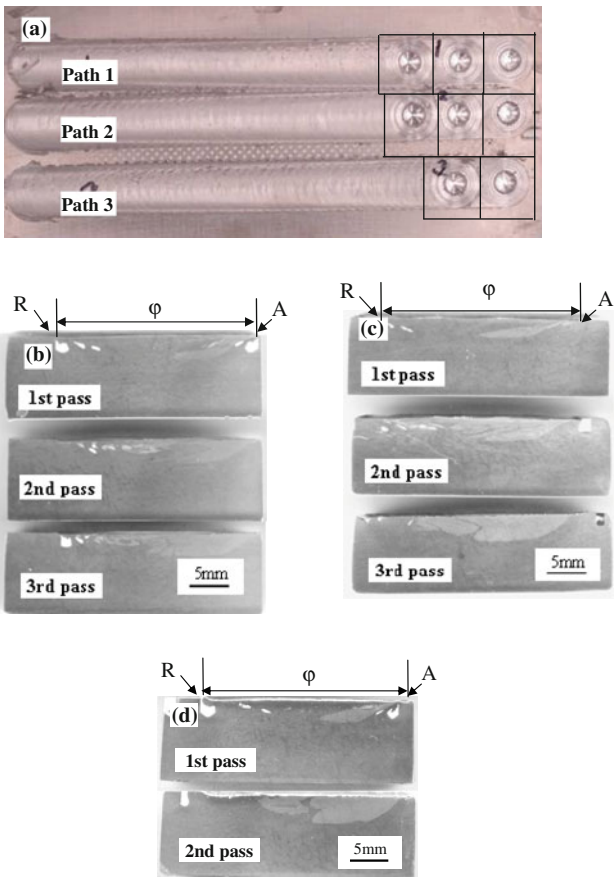

Fig. 5 Schematic of the locations of the cross section analyzed and OM images of the cross sections: **a** locations on the processed plate, **b** cross sections from Path 1, **c** Path 2, and **d** Path 3. R, Retreating side; A, Advancing side, φ, Shoulder diameter

amount of unmixed Al_2O_3 ceramic powders inside the FSP processed zone reduced with increase in number of passes. The axial force appears to have a significant effect on the formation of AMCZ. The depth of the AMCZ is about the same length of the pin of the tool.

The formation of AMCZ is from the material flow during the FSP. In the study of the material flow behavior during FSW [25, 26], it was observed that not all the material in the tool path was actually stirred but rather a large amount of the material was simply extruded around the retreating side of the welding tool pin and deposited behind. The only stirred material was at the top of the weld where the material transport was directly influenced by the tool shoulder which moves the material from the retreating side around the pin to the advancing side. Materials were also pushed downward on the advancing side and moved toward the top at the retreating side within the pin diameter. Material in the front of the advancing side of the tool entered into the mixing zone that rotates and advances simultaneously with the pin. The material in this zone was very highly deformed and sloughed off behind the pin in

arc shaped. Materials in front of the retreating side of the pin extrude between the rotational zone and base metal which in the wake of the weld fills in between materials sloughed off from the rotational zone. Therefore, the AMCZ appears at the advancing side in arc shape in the samples processed by the first pass.

Note that FSP has been demonstrated to be an effective means in refining grain size of cast or wrought aluminum-based alloys through dynamic recrystallization. Due to the refined grain size, aluminum-based alloy after FSP possesses better deformability. In our study, with the additional FSP passes, the plastic deformation within the thermo-mechanical affected zone increased, and the clustered or unmixed particles were broken and dispersed into matrix metal. Consequently, the amount of unmixed Al_2O_3 ceramic powder was reduced and the AMCZ region expanded as shown in Fig. 5b–d.

When a higher axial force is applied, the friction force between the shoulder/pin and the processed material is raised as a consequence. The temperature of the processed plate therefore increased as well. At higher temperature, material flows easier and the material on the advancing side was sloughed off wider (as can be seen from Fig. 5c, d). In summary, the axial force has significant effect on the formation of AMCZ, i.e., a larger axial force makes expanded AMCZ.

Microstructure

Figure 6 shows the optical microscopic images of AMCZ and the transition region from composite coating to aluminum alloy substrate. They are from samples along Path 1 after different passes with the same axial force of 17.64 kN. When the tool rotation rate, transverse speed, and axial force are kept constant, while the number of pass increases, the AMCZs are very well bonded to the aluminum alloy substrate. There is no apparent interface between the AMCZ and the substrate as shown in Fig. 6d–f. However, there are pores in the AMCZ and the transition region (i.e., the black dot in Fig. 6). With more FSP passes, the pores became smaller and distributed more evenly. As shown in Fig. 6a, after the first pass, the dispersion of Al_2O_3 particles within AMCZ is basically uniform. Some local inhomogeneous areas of particles can still be found in this sample.

Note that the as-received rolled aluminum alloy substrate plate has relatively large residual strain and stress from its manufacturing process which makes it difficult for the alloy to deform and flow during the first pass of the FSP. In this case, there are some large pores in both the AMCZ and the transition region (see Fig. 6a, d). However, during subsequent FSP passes, metal can deform and flow easier due to the softening of matrix material via dynamic

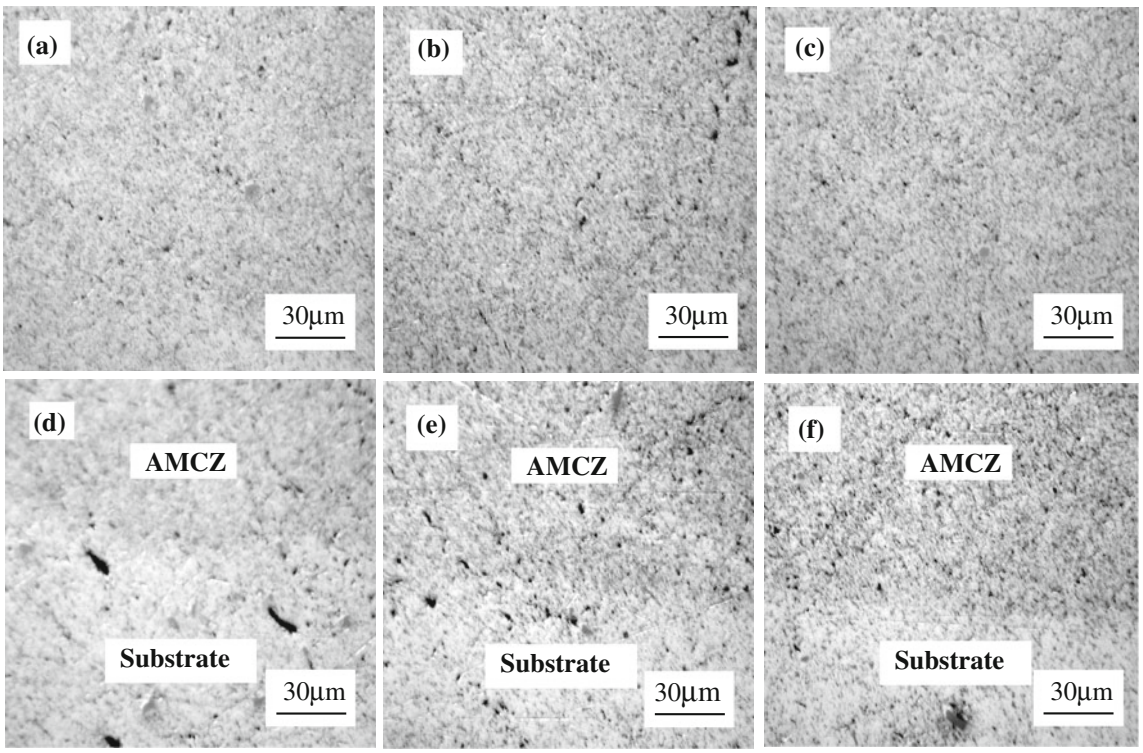

Fig. 6 Optical microscopic images of samples processed by different passes in AMCZ and transition region from composite coating to aluminum alloy substrate: **a** AMCZ after one pass; **b** AMCZ of two passes; **c** AMCZ after three passes; **d** transition region after one pass; **e** transition region after two passes; and **f** transition region after three passes (17.64 kN axial force)

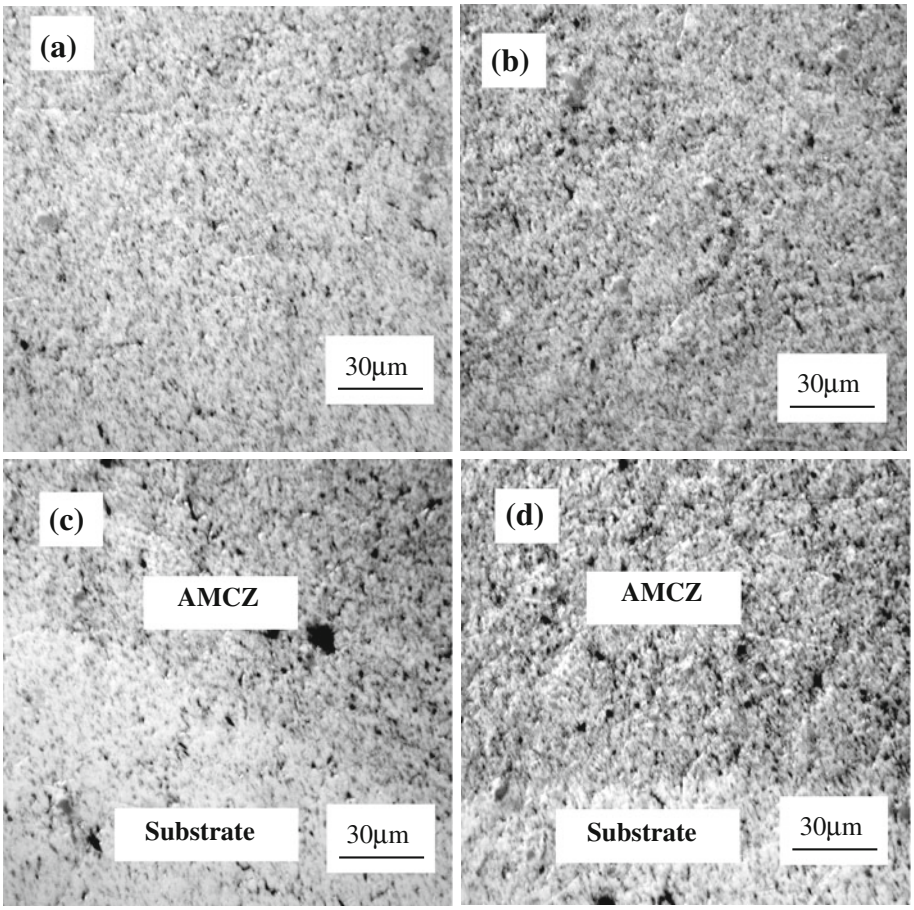

Fig. 7 Optical microscopic images of processed samples under different axial forces in AMCZ and transition region from composite coating to aluminum alloy substrate: **a** AMCZ under 17.64 kN; **b** AMCZ under 22.05 kN; **c** transition region under 17.64 kN; and **d** transition region under 22.05 kN (after two passes)

recrystallization and overage developed from the prior pass. So the pores turned into smaller size and disperse more uniformly. This can be seen by comparing Fig. 6a, d with b, c, e, and f.

The optical microscopic images of the cross section of the samples from Path 2 and Path 3 after processed by two passes under different axial forces are displayed in Fig. 7. It is evident that greater axial force resulted in relatively uniform dispersion of Al_2O_3 particles. This is because greater axial force causes greater friction force between the tool and the stirred material and higher temperature in the plate. Consequently, the plastic deformation of the material is more severe and stirred material flows easier that make uniform distribution of the Al_2O_3 particles in AMCZ.

Hardness measurements

Vickers hardness testing at the cross section of the FSP specimen was performed. The locations of the hardness tests and typical micro-hardness results are depicted in Fig. 8 with line (1) 0.6 mm below and parallel to the surface and line (2) from the top to the bottom of the plate. The micro-hardness distribution along line (1) shows that the scatter of hardness within AMCZ is minor, implying

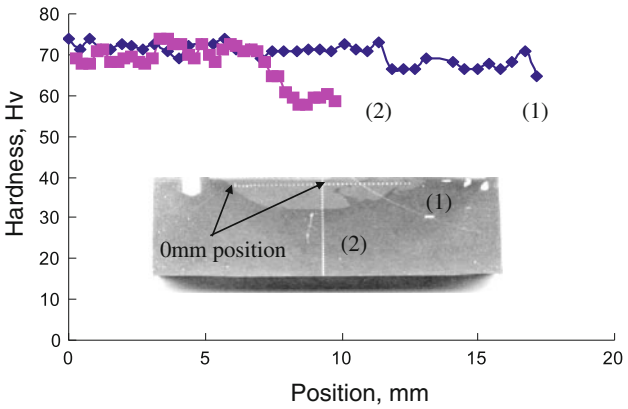

Fig. 8 Vickers hardness testing location and micro-hardness distribution in the base aluminum alloy and nano-composite zone of Path 2 after three passes

that the stirring by the pin efficiently dispersed the nano powders into a reasonably uniform manner. The micro-hardness distribution along line (2) shows that the AMCZ and FSZ have higher hardness values than other zones due to refined grain size via dynamic recrystallization. The lowest hardness is in the HAZ. Furthermore, it appears that adding in nano particles in the composite zone did not alter the micro-hardness of the base metal AA6061 aluminum

alloy. This is likely due to that the as-received 6061-T6 plate has been overaged after FSP because of the dissolution/coarsening of the precipitate. In this case, the increase in the hardness of the composite due to the addition of the ceramic particulates was countervailed by the softening of the matrix due to the overaging.

Torque

Figures 9, 10, and 11 show the spindle torques measured from the three FSP paths. The three paths contain different axial force in each pass as indicated in the figure. Figure 9 shows the spindle torque from Path 1 in which the axial force was kept constant at 17.64 kN. Despite the small, high frequency variation, the average spindle torque in Fig. 9a dropped from 12.23 to 10.89 N·m initially and then slowly increased to 11.78 N·m toward the end of the FSP. After processed by the first two passes, the average spindle torque in Fig. 9c has a large drop in the beginning and maintains relatively flat at about 10.5 N·m during pass 3. It appears that the spindle torque reduced slightly and stayed steadily with later passes.

By comparison of Fig. 9 with Fig. 10, it was observed that the spindle torque is steadier when the specimen was processed by more than one passes. However, the average spindle torque at steady state in each pass is different due to different axial force. The average spindle torque is 10.60 N·m in Fig. 9c and 11.01 N·m in Fig. 10c. The spindle torque curve in Fig. 11b has the similar profile to that in Figs. 9c and 10c, implying that at the increase of the passes the curve becomes steady. The average spindle torque in Fig. 11b is 11.59 N·m. The difference of spindle torque in Fig. 11b and in Fig. 10c indicates that the number of pass also has an influence on the value of spindle torque.

The material flow stress and friction force lead to the development of the spindle torque as the work piece material resists tool rotation. It is well known that friction force between two surfaces is equal to the product of normal force and friction coefficient. Colligan and Mishra [27] has constructed a conceptual model for the process variables related to heat generation in friction stir welding of aluminum and observed that the measured spindle torque depends on friction coefficient between surfaces, normal force, and shoulder radius of tool, i.e., $M_e = 2/3\mu F_z R$, where M_e is the spindle torque, μ is the friction coefficient between surfaces, F_z is the normal force, and R is the shoulder radius of the tool. Material flow in the processed zone is influenced by the extrusion process, where the applied axial force and the motion of tool pin propel the material after it has undergone the plastic deformation. Krishnan [28] has studied the mechanism of onion ring formation in the friction stir welds of aluminum alloys and found that the degree of material mixing and inter-diffusion, material flow patterns, and material flow stress depend on the axial force. It is apparent that the spindle torque would increase with increasing axial force.

As heat treatable alloy, the matrix material has been softened due to overaging after FSP because of the dissolution/coarsening of the precipitate. Thus, the deformation of metal becomes easier and the material flow stress

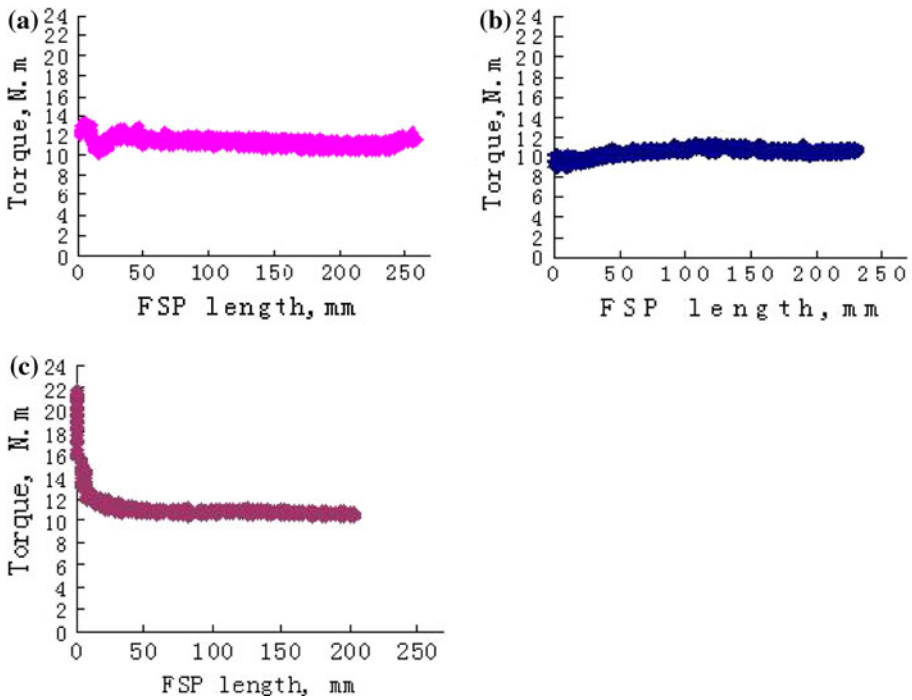

Fig. 9 Spindle torque of Path 1 during **a** 1st pass; **b** 2nd pass; and **c** 3rd pass with a constant axial force 17.64 kN

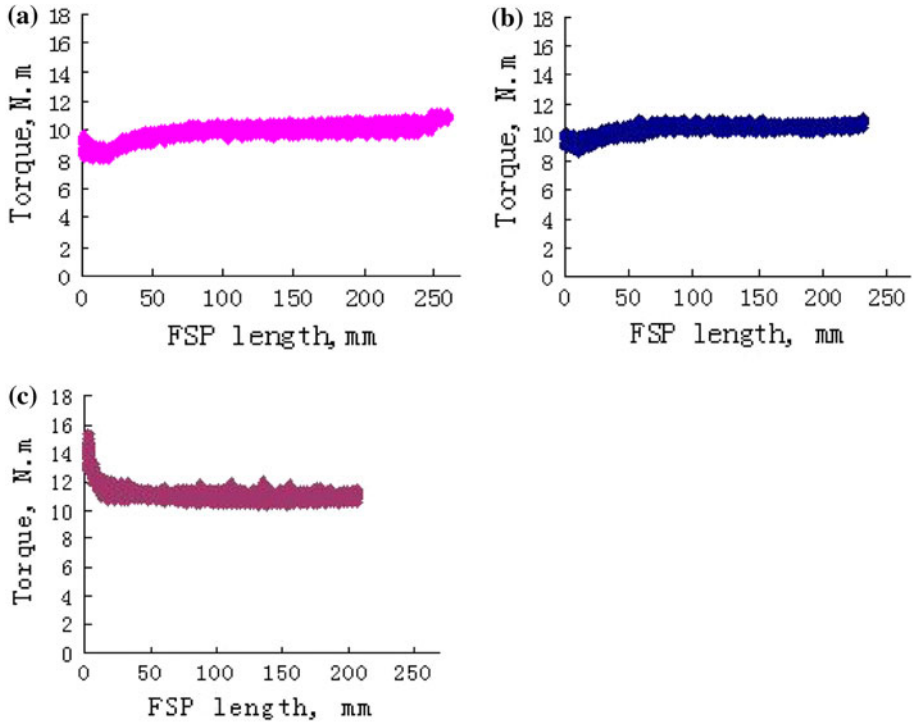

Fig. 10 Spindle torque of Path 2 processed by different axial forces in each passes: **a** 1st pass at 13.23 kN; **b** 2nd pass at 17.64 kN; and **c** 3rd pass at 22.05 kN

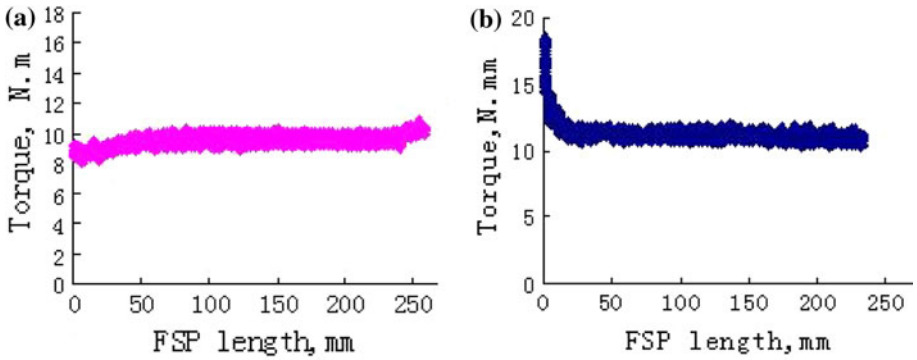

Fig. 11 Spindle torque of Path 3 during **a** 1st pass with axial force 13.23 kN; and **b** 2nd pass with axial force 22.05 kN

reduced with increasing number of pass. In addition, the distribution of the ceramic particles in the friction stirred zone became more homogeneous as shown in Figs. 5, 6, 7. Result in reference [19] had proved that adding ceramic nano particles into metal can reduce the friction coefficient of metal. As a result, the friction force between surfaces is reduced. Furthermore, the spindle torque was decreased and became steadier with additional FSP passes.

Conclusion

Several conclusions can be made through this FSP study:

(1) The composite zone developed as deep as the length of the pin probe. No interface was developed between the composite zone and the base metal. The composite zone became larger when axial force and the number of pass are increased.

(2) The distribution of the ceramic particles in the composite zone is more homogeneous with the increase of number of FSP pass and axial force.

(3) Nano particles have no distinct effect on the macrohardness of AA6061-T6 aluminum alloy even in the composite zone due to the softening of matrix material resulted from overaging.

(4) Spindle torque (a) increased with increasing axial force, and (b) became less variable and smaller during subsequent passes in multiple pass FSP.

Acknowledgements The authors would like to thank Dr. Wei Tang and Mr. Dan Wilhelm of the Department of Mechanical Engineering, University of South Carolina for their help in the FSP.

References

1. Elmadagli M, Perry T, Alpas AT (2007) Wear 262:79
2. Qu J, An L, Blau PJ (2006) Proceedings of IJTC2006 STLE/ASME international joint tribology conference, San Antonio, Texas, p 59
3. Cavaliere P (2005) Compos Part A Appl Sci Manuf 36:1657
4. Ceschini L, Boromei I, Minak G, Morri A, Tarterini F (2007) Compos Part A Appl Sci Manuf 38:1200
5. Dong S, Han J, Du S, Wang M (1999) Mater Sci Technol 7:28
6. Zhang J, Tian Z, Zhao J (2004) Laser J 25:67
7. Singh H, Puri D, Prakash S, Hira DS (2007) Mater Sci Technol 23:736
8. Almeida A, Vilar R (2008) Lasers Eng 18:49
9. Jiang B, Xu B, Dong S, Wang H (2002) Cailiao Baohu 35:1
10. Bakshi SR, Singh V, Balani K, McCartney DG, Seal S (2008) Surf Coat Technol 202:5162
11. Mishra RS, Ma ZY, Charit I (2003) Mater Sci Eng A 342:307
12. Ma ZY, Mishra RS (2003) Surface engineering: in materials science II, TMS, p 243
13. Ramadorai U, Newkirk JW, Mishra RS (2005) Proceedings of the 19th international conference on surface modification technology, Minnesota, p 22
14. Mahmoud ERI, Ikechi K, Takahashi M (2008) Sci Technol Weld Joining 13:607
15. Lee CJ, Huang JC, Cu XH (2007) Mater Trans 48:780
16. Chang CI, Wang YN, Pei HR et al (2007) Key Eng Mater 351:114
17. Chang CI, Wang YN, Pei HR et al (2007) Mater Trans 47:2942
18. Shafiei-Zarghani A, Kashani-Bozorg SF, Zarei-Hanzaki A (2009) Mater Sci Eng A500:84
19. Qu J, Xu H, Feng Z, An K et al (2009) Trans NAMRI/SME 37:349
20. Morisada Y, Fujii H, Nagaoka T, Fukusumi M (2006) Mater Sci Eng A 433:50
21. Morisada Y, Fujii H, Nagaoka T, Fukusumi M (2006) Scr Mater 55:1067
22. Lim DK, Shibayanagi T, Gerlich AP (2009) Mater Sci Eng A 507:194
23. Wang W, Shi Q, Liu P, Li H, Li T (2009) J Mater Process Technol 209:2099
24. Elangovan K, Balasubramanian V (2008) Mater Des 29:362
25. Reynolds AP (2008) Scr Mater 58:338
26. London B, Mahoney M, Bingel W, Calabrese M, Bossi RH, Waldron D (2003) TMS annual meeting, friction stir welding and processing II, p 3
27. Colligan KJ, Mishra RS (2008) Scr Mater 58:327
28. Krishnan KN (2002) Mater Sci Eng A 327:246